Monte-Carlo toolkit for designing and validating Step-Range-Filter spectrometer designs

T. M. Johnson,[1, a)] B. Lahmann,[1, 2] L. Russell,[1] N. L. Vanderloo,[1] M. J. Cufari,[1] B. L. Reichelt,[1] C. W. Chang,[1] A. Birkel,[1] N. V. Kabadi,[1, 3] G. D. Sutcliffe,[1, 2] P. J. Adrian,[1, 4] J. A. Pearcy,[1] J. H. Kunimune,[1] S. G. Dannhoff,[1] T. E. Evans,[1] M. Gatu Johnson,[1] F. H. Séguin,[1] R. D. Petrasso,[1] C. K. Li,[1] and J. A. Frenje[1]

[1)]*Massachusetts Institute of Technology, Cambridge, Massachusetts 02139, USA*

[2)]*Lawrence Livermore National Laboratory, Livermore, California 94550, USA*

[3)]*Laboratory for Laser Energetics, University of Rochester, Rochester, New York 14623, USA*

[4)]*Los Alamos National Laboratory, Los Alamos, New Mexico 87545, USA*

(Dated: 30 January 2025)

Here, we present a Monte-Carlo toolkit for validating step range filter (SRF) spectrometer designs. Geant4 is used to transport charged particles through the SRF filters to generate synthetic SRF data which include realistic CR-39 effects. Synthetic SRF spectra generated by this method inherently account for instrument response and allow for the quantification of SRF performance before shots. The usefulness of this toolkit is demonstrated through its application to a number of problems. A new broadband SRF for the ∼10 MeV wide ^{3}He^{3}He proton spectrum is validated and an analysis method for analyzing ^{3}He^{3}He-p SRF data that accounts for instrument response is put forth. In addition, an SRF design for the compact recoil-proton spectrometer (CRS) on the Z-machine is validated. Lastly, a new calibration technique for the DD-p SRF is proposed and validated.

I. INTRODUCTION

Step range filter (SRF) spectrometers are used at inertial confinement fusion (ICF) facilities to measure charge particle spectra at lower energies, down to about 2 MeV[1,2]. The wedge-range-filter (WRF), a commonly used proton spectrometer, is typically limited to energies above around 6 MeV[3]. For this reason, SRFs are commonly used to measure DD-p spectra (mean energy of 3 MeV). The modular design of the SRF allows the extension of its capability by adding additional filters.

The limitation of the WRF is apparent in previous work done to measure the ^{3}He^{3}He-p spectrum[4]. In these experiments, the WRF was able to measure this spectrum down to 6 MeV, showing good agreement with two different *R*-matrix models[4]. These models do not agree below 6 MeV, which motivates the use of an SRF to measure this part of the spectrum. Previous work proposed an SRF design to make this measurement, but this discussion lacked a technique for validation[2].

Here, we present a Monte-Carlo toolkit for validating and exploring the instrument response of different SRF designs. Validation is the process of showing that a certain SRF design is able to measure the charged particle spectrum of interest over a wide range of realistic conditions. This toolkit uses Geant4 to model the physics of particles passing though the SRF filters[5–7]. The Geant4-generated energies of the particles are converted into particle tracks on CR-39 and realistic variations in track diameters (resulting from the CR-39 scan) are applied. These diameters are then fed into the SRF analysis program to find a synthetic SRF spectrum, which can be used to predict the performance of an SRF design.

This Monte-Carlo toolkit is used to validate a proposed SRF design for measuring the ^{3}He^{3}He-p spectrum. The Monte-Carlo toolkit is also applied to validate an SRF configuration for the DD neutron compact recoil-proton spectrometer (CRS) on the Z-machine[8]. An SRF is needed to find the quantitative relationship between energies and track diameters of the DD neutron recoil protons on the CR-39 detector[3]. Once this relationship is found, the recoil-proton spectrum can be reconstructed. Due to the low mean energy (about 2 MeV) of the recoil spectrum, a special SRF design is required. In addition to validation, the Monte-Carlo toolkit is used to study other aspects of the SRF. Issues have occurred with performing the DD-p SRF calibrations[2]. X-ray calibrations were preformed and the results used to analyze OMEGA DD-p proton spectra. The Monte-Carlo toolkit inherently applies the instrument response function to synthetic spectra. This fact was used to remove the instrument response from OMEGA DD-p spectra enabling the comparison to other charged particle spectrometers.

This paper is organized as follows. Section II summarizes the SRF as a diagnostic. The Monte-Carlo code is detailed in section III. The model is applied to the ^{3}He^{3}He-p spectrum in section IV, where a new SRF design is validated and an analysis method for analyzing data is put forth. A design for an SRF for the CRS spectrometer is validated in section V. The standard calibration is explored for the DD-p SRF in section VI. The work is summarized in section VII.

II. SRF DESIGN

The design of the SRF spectrometer is based on overlapping metal foils, called filters, of different thicknesses[2]. The regions where the filters overlap are called windows. Each window looks at a particular part of the charged particle spectrum. This works because each window functions as a range filter to slow down the protons by different amounts. The overlapping of the filters allows for a relatively small num-

[a)]tmarkj@mit.edu

ber of filters to make a large number of windows. Fig. 1 B) shows this schematically. A filter thickness calibration is used to determine the thickness of the filters, which in turn set the thickness of the windows without the need of calibrating each window individually[2].

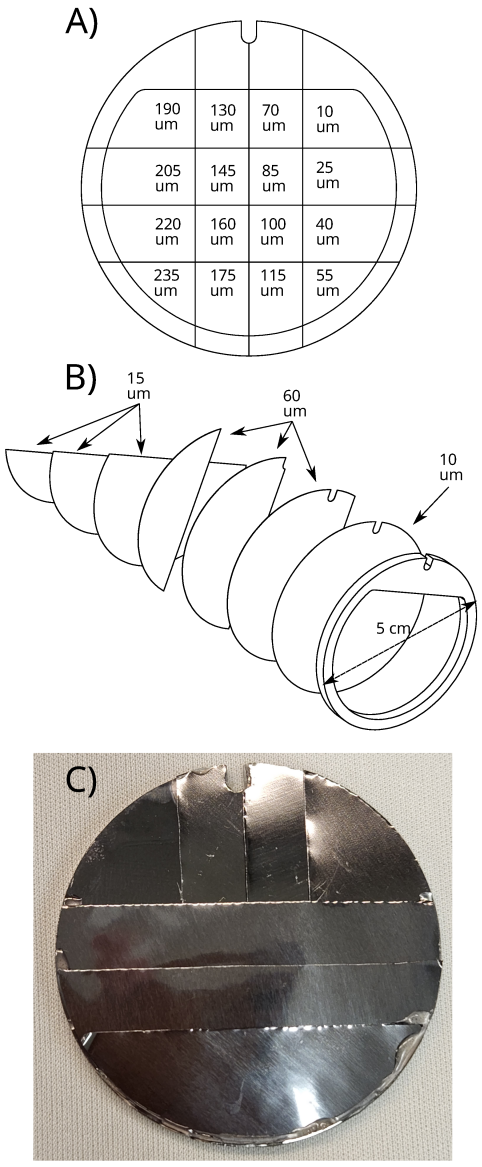

FIG. 1. A) Schematic of the new compact SRF spectrometer design. Sixteen windows are incorporated in the design, with Ta windows ranging from 10-235 μm in steps of 15 μm. The SRF has an outer diameter of 5 cm. The outer frame of the SRF is 1.5 mm thick Al, which ranges out all protons below about 16.5 MeV. B) Exploded view of the SRF filter arrangement showing how the seven different filters overlap to create sixteen windows. The base filter is 10 μm thick while the horizontal and vertical filters are 15 μm and 60 μm thick, respectively. C) Photo of the backside of the SRF showing the overlapping Ta filters.

The SRF uses a CR-39 detector to measure charged particle spectra[3]. Charged particles passing through the CR-39 material leave trails of molecular damage. Etching the CR-39 in a 6M NaOH solution reveals particle tracks whose size depends on the amount of energy the particle lost while interacting with the detector. High energy particles do not lose much energy per unit distance in the CR-39 so they leave small diameter tracks. Low energy particles, closer towards the Bragg peak, lose a large amount of energy per unit distance and therefore leave large tracks. The exact relationship between particle energies and track diameters varies between pieces of CR-39 and is explained by the single variable c-parameter model:

$$D(E) = 1.2\exp\left[-\frac{E-1}{0.3}\right] + 11.3\exp\left[-\frac{E-1}{3.0}\right] + 4.8\exp\left[-\frac{E-1}{8.0}\right] \quad (1)$$

$$D_c = \begin{cases} \begin{cases} 20\exp(-c|\log(D/20)|) & D \le 20 \\ 40 - 20\exp(-c|\log(D/20)|) & D > 20 \end{cases} & c < 1.0 \\ \begin{cases} \frac{(20-D)^2}{20-2D}\left[e^{\frac{c}{2}\log[\frac{D^2}{(20-D)^2}]} - 1\right] + 20 & D \le 10 \\ 20 - c(20-D) & D > 10 \end{cases} & c > 1.0 \end{cases} \quad (2)$$

where E is the proton energy in MeV, D is the track diameter on the CR-39 in μm, c is the fitting parameter called the c-parameter, and D_c is the resulting diameter given c[3,9,10]. Values of the c-parameter typically range from 0.8 to 1.6. Fig. 2 shows plots of diameters vs energy for different values of c. The model shown in equation 2 is valid for diameters that have been scaled to account for the increase in diameters caused by etching (see appendix B in reference[10]). Previous work has shown that the c-parameter model accurately describes the relationship between particle track diameter and particle energy[10].

The SRF analysis procedure works as follows[2]. For each value of c-parameter in a list, diameter distributions are converted into energy spectra for each SRF window. These energy spectra are then reversed-ranged through the thickness of the window using SRIM generated ranging tables[11]. Since all the SRF windows are exposed to the same input spectrum, the reconstructed spectra from each of the windows should agree with one another. The correct value of the c-parameter is determined by finding c where this agreement is maximized. This analysis procedure assumes that the c-parameter is constant across the piece of CR-39 which has been shown to be a good assumption[2]. The spectrum reconstructed from this analysis is convolved with the instrumentation response function. This spectrum will herein be referred to as the uncorrected spectrum. In order to obtain precise information about the source spectrum, the instrument response needs to be considered.

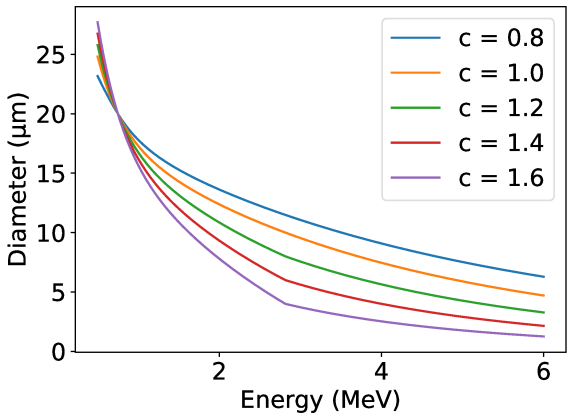

FIG. 2. Plot of the relationship between track diameters and particle energies for different values of the c-parameter. Note that plots of with $c > 1$ have a kink 2.81 MeV. This is because, at this energy, equation 1 gives has a diameter of exactly 10 μm which results in equation 2 moving to the $D > 10$ case.

III. MONTE-CARLO TOOLKIT

The goal of the SRF Monte-Carlo toolkit is to generate a synthetic uncorrected SRF spectrum for a given input proton spectrum and is built around Geant4. The Geant4 toolkit is used to model the passage of protons through the thin SRF filters of either tantalum or aluminum[5–7]. The simulation setup for Geant4 consists of a single filter. Particles generated at a point source are launched in a straight line toward the filter. The energy of the particle is recorded immediately behind the filter. Geant4 uses a single scattering Coulomb model to capture elastic scattering of the protons off the material. Elastic scattering causes the proton to deviate from a straight trajectory which results in it traveling through more material causing more energy loss. This phenomenon is known as energy straggling[2]. By default, Geant4 uses a Bethe-Bloch model for stopping power. In order to improve the accuracy of Geant4, it was modified to use SRIM tables for the stopping power calculation[11]. The SRIM modified version of the `emstandardSS` Geant4 physics list is used since it explicitly models single scattering Coulomb collisions for energy straggling. Validation of the modified Geant4 stopping power is presented in appendix A.

The SRF Monte-Carlo toolkit works as follows. Geant4 is used to expose each SRF window of different thickness to the input proton spectrum. The energy of the protons leaving the foil are recorded. These energies represent the energy of the protons going into the CR-39. The energy distribution for each SRF window is then converted into track-diameter distributions by assuming a value of the c-parameter. An effect, called diameter blurring, is applied to the diameters in order to account for the variation in track diameters that arises during the CR-39 microscope scanning process[2]. This effect slightly varies the measured value of the particle track diameters from the actual values[3]. This results in the distribution of scanned diameters being wider than the true distribution on the CR-39. Previous work has shown that this effect blurs the diameters by $\sigma_{\text{blur}}/D = 8.1 \pm 0.5\%$[2]. Previous work also found this to be the most important broadening mechanism for SRFs[2]. With each window having a unique diameter distribution, the SRF analysis procedure, described in section II, is applied to the set of diameter distributions to solve for the synthetic SRF spectrum. This synthetic uncorrected SRF spectrum can be used for a number of purposes. Synthetic uncorrected SRF data naturally encodes the instrument response function due to the inclusion of the diameter blurring and the use of the SRF analysis procedure. Fig. 3 shows a clarifying flow chart of how the Monte-Carlo toolkit works. This paper details several examples of different ways to use the output from the Monte-Carlo toolkit to answer important questions about SRF designs.

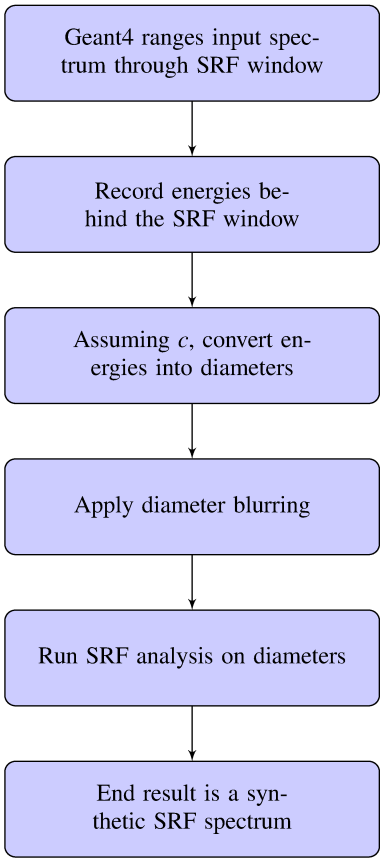

FIG. 3. Diagram describing the Monte-Carlo model. The first four steps generate a set of diameters for each window of the SRF. These diameters are then analyzed using the normal SRF analysis procedure. The result is a synthetic SRF spectrum.

This tool is powerful in that it provides a way to validate new SRF designs before building them and using them in an actual experiment. Fig. 4 shows agreement between a real uncorrected accelerator spectrum and the uncorrected synthetic data for a 9-window DD-p proton SRF with data behind the nominally 10 μm, 15 μm, and 20 μm thick windows[12]. These data were generated using an electrostatic ion accelerator to collide a 125 keV deuterium beam into a ErD_2 target

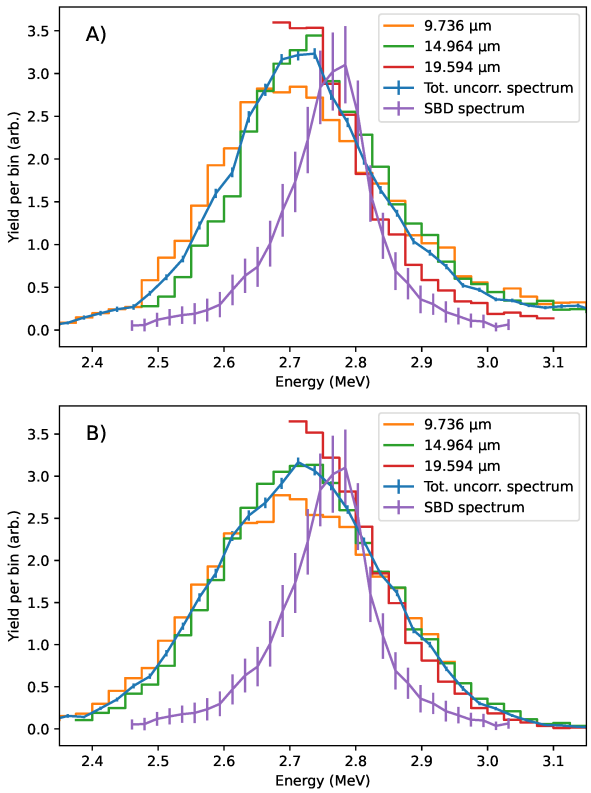

FIG. 4. A) An uncorrected DD-p SRF spectrum collected at the MIT linear electrostatic ion accelerator. The blue plot shows the total uncorrected SRF spectrum while the other colors show the individual window spectra. Counting statistics and diameter blurring are responsible for the mismatch between the window spectra. The c-parameter was found to be 1.07. B) Synthetic uncorrected SRF spectrum with similar inputs as the accelerator data. In blue is the total uncorrected SRF spectrum while the other colors show the individual window spectra. Note that the synthetic data captures several features of the real data. The uncorrected peak energies of the spectra are very close, 2.74 ± .025 MeV in A) and 2.71 ± .025 MeV in B). The way in which the individual window spectra overlap is similar between the accelerator and synthetic spectra. The spectrum inferred by the thickest filter in both data sets has too much fluence at lower energy then too little fluence at high energy. This is due to variation in the particle track diameter size from diameter blurring and the shape of the c-parameter model curve. In both A) and B), the uncorrected SRF spectra are shifted from the SBD spectrum due to the instrument response function.

to produce DD-p protons[12]. A silicon surface barrier detector (SBD) was used to measure the incident DD-p proton spectrum which was used to generate the synthetic data in Fig. 4. The agreement is both qualitative and quantitative with the real and synthetic uncorrected spectra having very similar peak energies. This comparison is valid because the instrument response function is applied to both datasets.

Since Geant4 allows for arbitrarily shaped input spectra, the SRF Monte-Carlo toolkit is able to generate synthetic SRF spectra for any input spectrum. This is essential for studying broad spectra, such as the ^{3}He^{3}He-p spectrum as described in the next section.

IV. ^{3}HE^{3}HE-P PROTON SRF

Measurements of the ^{3}He^{3}He-p spectrum have been made using HED plasmas at the OMEGA laser facility for proton energies above ∼6 MeV[4]. It was found that a good fit to the experimental data could be obtained by varying the *R*-matrix feeding factors[4]. Model 1 was generating by translating the *R*-matrix model from TT accelerator measurements and varying the feeding factors[13]. Likewise, model 2 was generated by translating the *R*-matrix model from TT fusion experiments at the National Ignition Facility and varying the feeding factors[14,15]. As the different *R*-matrix models of the ^{3}He^{3}He-p spectrum differ from each other at lower proton energies, a new spectrometer capable of measuring the low-energy part of the spectrum should be developed[4]. Previous work has put forth an SRF design for measurements of the ^{3}He^{3}He-p spectrum[2]. This spectrometer does not have enough energy overlap to robustly measure the broad-band ^{3}He^{3}He-p spectrum. A new SRF design for measurements of the ^{3}He^{3}He-p spectrum was developed and validated by the SRF Monte-Carlo toolkit. This new design can robustly measure the entire ^{3}He^{3}He-p spectrum for a wide range of c-parameters. An analysis method is also put forth for determining which model ^{3}He^{3}He-p spectrum best matches the measured spectra. In addition, the effect of poorly characterized filter thicknesses is studied and a required SRF calibration accuracy for the measurement of the ^{3}He^{3}He-p spectrum found.

The SRF Monte-Carlo toolkit is applied to a new SRF design for measurement of the ^{3}He^{3}He-p spectrum. The new SRF design has a total of 16 windows made by overlapping 7 different tantalum filters. The base filter of the new design is 10 μm and the window thickness step size is 15 μm. The additional windows provide more energy overlap than the 9 window design while providing enough statistics for low-yield reactions such as the ^{3}He^{3}He-p reaction[2,4]. Fig. 1 shows a schematic of the new SRF design. Appendix B compares the Monte-Carlo toolkit predicted performance of the new SRF design compared to the older 9 window design and finds that the new design outperforms the old one.

TABLE I. Reduced χ^2 values for different comparisons between the *R*-matrix SRF spectra and the low fluence surrogate experimental spectra as shown in Fig. 5 C). Even at low fluence, the χ^2 technique is clearly able to determine which model generated it.

	Model 1 response	Model 2 response
Model 1 surrogate exp.	1.621	3.226
Model 2 surrogate exp.	4.340	1.112

The SRF Monte-Carlo toolkit was used to generate synthetic uncorrected ^{3}He^{3}He-p spectra as shown in Fig. 5 A) and B). Comparing the *R*-matrix model uncorrected spectra directly to the measured spectra is complicated by the instrument response which results in a shift of the high energy resonance peak as seen in Fig. 5 A) and B). This response effect

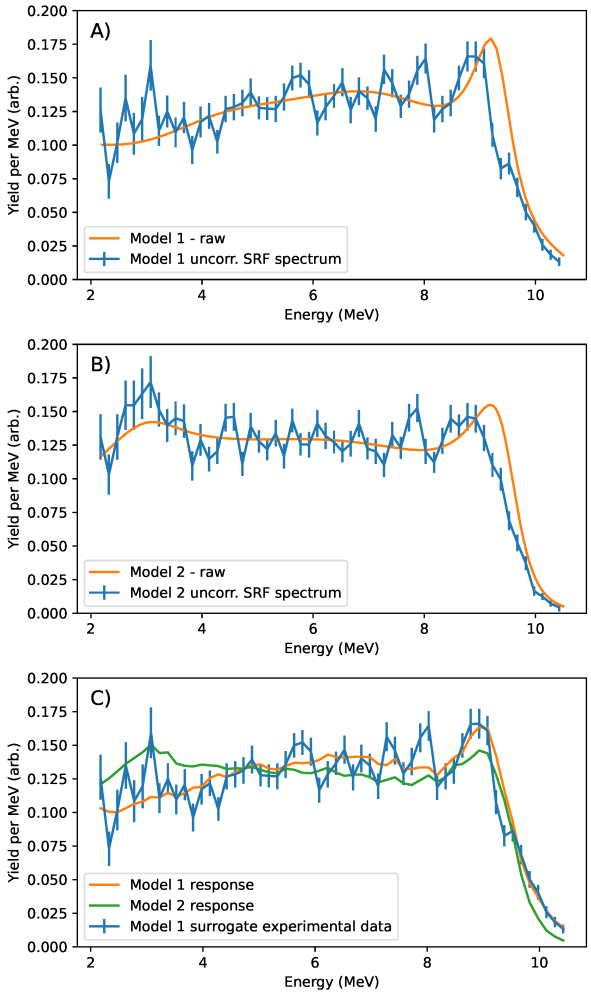

FIG. 5. A) Synthetic uncorrected SRF spectrum generated with the model 1 *R*-matrix spectrum in blue and the raw model 1 *R*-matrix spectrum in orange. Notice that the SRF instrument response function shifts the high energy resonance peak to lower energy. B) Synthetic uncorrected SRF spectrum generated with the model 2 *R*-matrix spectrum and the raw model 2 *R*-matrix spectrum. C) Surrogate experimental data generated with the model 1 *R*-matrix spectrum at realistic low fluence of 3600 tracks per cm^2 in blue alongside synthetic model 1 and model 2 response spectra in orange and green, respectively.

needs to be considered in the analysis. In principle, one could generate a response matrix of energy shifts and broadening caused by the SRF, as done in previous work[2]. However, this effort is complicated by the variable nature of the energy shift as discussed in appendix C.

The goal of analyzing ^{3}He^{3}He-p SRF data is to determine which *R*-matrix model best explains the measurement. A better and simpler approach than removing the response is to the use the SRF Monte-Carlo toolkit to apply the response to the *R*-matrix models. This is done by using the *R*-matrix models as input to generate synthetic spectra at very large number of particles to produce sufficient convergence to the "true" response spectrum. These spectra are referred to as the response spectra. The same parameters, c-parameter and filter thicknesses, as in the experiment should be used to generate the response spectra to keep the instrument response the same. Fig. 5 C) shows the comparison between the realistically low statistics (3.6×10^3 tracks per cm^2) surrogate experimental spectrum, generated from the model 1 *R*-matrix spectrum, and the response spectra. The response spectra are generated at high fluence (3.6×10^5 tracks per cm^2) with either the model 1 or the model 2 *R*-matrix spectra as the input proton spectrum. A reduced χ^2 method is used to compare the surrogate experimental data to the response spectrum. Table I shows the corresponding reduced χ^2 values from this comparison. Note that even for the low statistics of the surrogate experimental data, this analysis method successfully differentiates between the *R*-matrix models.

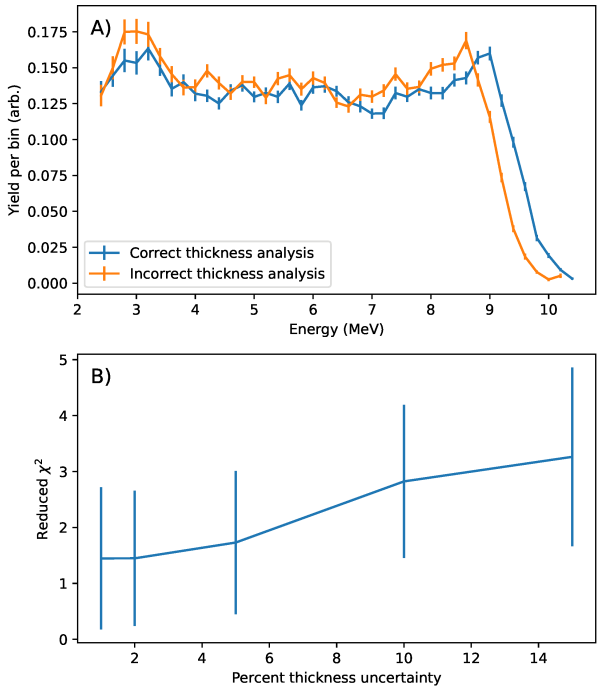

FIG. 6. A) A synthetic uncorrected ^{3}He^{3}He-p SRF spectrum that is generated with a randomly varied set of filters but analyzed with the nominal, and incorrect, window thicknesses compared to another synthetic uncorrected ^{3}He^{3}He-p SRF spectrum generated and analyzed by using the correct window thicknesses. B) Reduced χ^2 for the analysis of SRF spectra generated with varied filters and analyzed with the nominal, and wrong, window thicknesses compared to the SRF spectrum generated with the nominal window thicknesses. The error bars describe the distribution of reduced χ^2 values formed by 100 repeated generations of new filter thicknesses with the same percent variation. Below about 5% precision in filter thickness gives diminishing returns in the χ^2.

When measuring DD-p spectra with SRFs, an erroneous width can be inferred when analyzing the data with wrong filter thicknesses[2]. With broad-band spectra, like the ^{3}He^{3}He-p spectrum, problems with using uncalibrated thicknesses are exacerbated. Fig. 6 A) shows an uncorrected ^{3}He^{3}He-p SRF spectrum generated with the SRF Monte-Carlo toolkit where

the analysis was done with an incorrect set of thicknesses generated by varying the filter thicknesses by 15%. Note that the energy of the rising edge of the high energy resonance peak is distorted. This effect can complicate the analysis of the spectrum and the determination of the *R*-matrix model spectrum. The metal foils used to build the SRFs usually have a thickness uncertainty of about 15% as stated by the manufacturer. An x-ray measurement technique is recommended to calibrate each individual filter thickness of the SRFs for an accurate measurement of the ^{3}He^{3}He-p spectrum[16]. Fig. 6 B) shows that the calibration needs to be done with a precision of 5% or better to avoid the issues described here.

V. CRS RECOIL PROTON SRF

The CRS spectrometer is a recoil DD-p neutron spectrometer on the Z machine which uses CR-39 as the detection medium[8]. Compared to other recoil neutron spectrometers, CRS does not use magnets for energy dispersion[17,18]. Instead, the CR-39 directly records the DD neutron recoil proton spectrum. Without additional information to constrain the c-parameter, the diameter distribution from the CR-39 cannot be used. An SRF was designed for this purpose. The CRS SRF consists of two regions: the unfiltered region and the SRF region. An image of this can be seen in Fig. 7 A). The small SRF region is designed to constrain the c-parameter for the piece of CR-39. Once the c-parameter has been found, the diameters in the unfiltered region can be converted into a recoil proton spectrum. Note that the downscatter part of the spectrum is at particularly low proton energy, which means that the SRF itself is not able to consistently reconstruct this part of the spectrum (protons from this part do not penetrate the SRF filters). The SRF is a fundamental part of the CRS spectrometer because it enables the reconstruction of the entire recoil proton spectrum.

MCNP simulations show that the CRS recoil proton spectrum has a relatively low mean energy of about 2 MeV[8]. Standard Ta SRFs will not work for this design since the spectrum is too low in energy. A new SRF design based on thin aluminum filters is used. The SRF has four windows with thicknesses of 6 μm, 12 μm, 18 μm, and 24 μm Al. Aluminum was chosen as the filter material to allow for less ranging than Ta in an easily available thickness. The SRF Geant4 Monte-Carlo toolkit is used to validate this design. The MCNP simulated spectrum was used as the input spectrum to the model. An example uncorrected spectrum is shown in Fig. 7 B)[8]. It was found that the chosen CRS SRF design works for diagnosing this type of spectrum for a wide range of c-parameters. The spectrometer also resolves the spectrum for realistically low fluences. Real data taken from the HEDP accelerator at MIT is shown in Fig. 7 C)[12]. The accelerator DD-p were downranged to relevant energies using a filter of 10 μm Ta. Protons were used instead of DD-n recoil protons to avoid issues with conversion efficiency and differences in the detector geometry. As expected, the SRF analysis converges in an energy range similar to the expected CRS proton energy range. The design and optimization of the CRS SRF was guided by using the SRF Monte-Carlo toolkit.

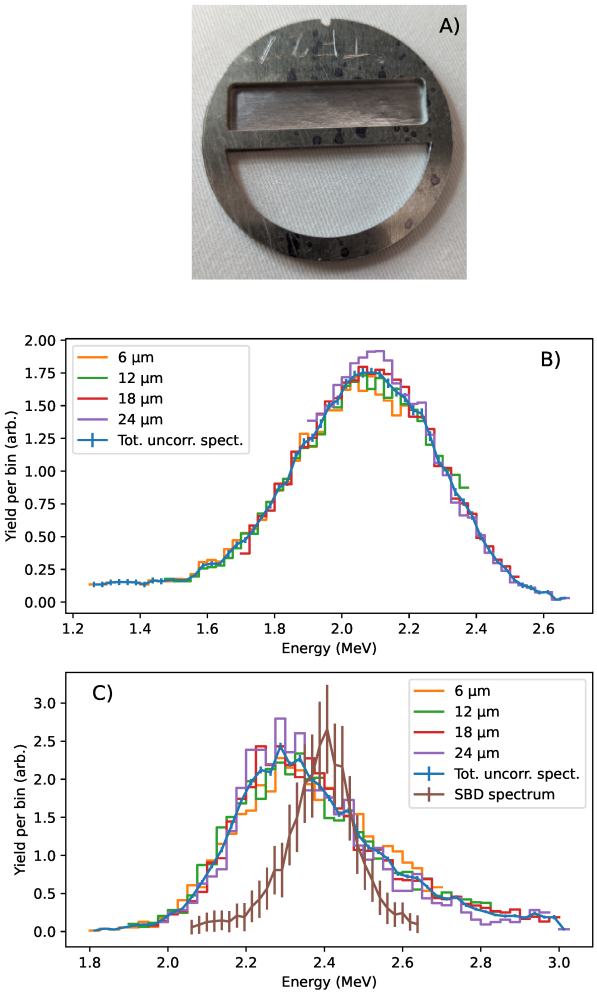

FIG. 7. A) The CRS SRF. The upper region with the aluminum filters is the SRF region of the detector. Below an unfiltered region exists which allows for the measurement of low energy recoil protons. B) Synthetic uncorrected CRS SRF recoil-proton spectrum generated with $c = 1.4$. The choice of aluminum filtering is shown to resolve the recoil proton spectrum. C) Example of an uncorrected CRS SRF downranged DD-proton spectrum generated with the HEDP accelerator. A 10 μm Ta filter was used to bring the DD proton spectrum into the energy range of the CRS SRF. The instrument response can be seen when comparing the SBD spectrum to the SRF spectrum

VI. DD-P PROTON SRF

The original technique for determining the thicknesses of the SRF filters was to use an accelerator[2]. The SRFs were exposed to DD protons at different lines-of-sight to record spectra at different energies. These data were then compared to SBD energy measurements. For the correct filter thicknesses, the SRF measured mean energy should match the SBD value after removing the instrument response. This technique is labor-intensive and has had some reliability issues which mo-

tivate the development of a new calibration technique.

Previous work has shown that x-ray transmission can accurately measure the thicknesses of thin metal foils used for high energy density physics applications[16]. This alternative calibration technique was applied to a set of DD-p SRFs. Four of the filters for each SRF were exposed to radiation from a titanium x-ray tube set to 25 kV. The resulting spectrum had a characteristic Ti k-α line and a bremsstrahlung tail. The net x-ray transmission curve was fit to determine the thickness of the tantalum filter.

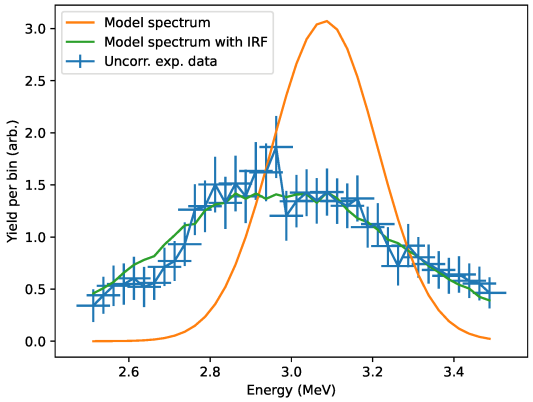

FIG. 8. Comparison between the uncorrected experimental DD-p proton spectrum from shot number 3 and the results from the Markov Chain Monte-Carlo analysis. The forward fit spectrum shown in the orange does not have the instrument response function applied and serves as the input to the Monte-Carlo toolkit. The spectrum in green is the forward fit spectrum with the instrument response function applied and agrees well with the uncorrected experimental data.

Using the thus inferred filter thicknesses, SRF data from DT implosions at OMEGA were analyzed and compared to a magnetic charged particle spectrometer (CPS)[3,19]. Table II shows the comparison between the calibration SRF and CPS measured mean energies. The Monte-Carlo toolkit is used here to remove the instrument response and allow for a direct comparison between SRF and CPS measured mean energies. This is done using a Markov Chain Monte-Carlo (MCMC) technique which utilizes the Monte-Carlo toolkit to forward fit a Gaussian to the uncorrected SRF spectrum. Each iteration of MCMC generates a synthetic uncorrected SRF spectrum with varied model inputs which is compared to the experimental uncorrected spectrum using a χ^2 likelihood. The results of this MCMC forward fitting are shown in Table II. A comparison between the experimental data and the forward fit MCMC results are shown in Figure 8. Both diagnostics agreed on the measured DD-p mean energies. This demonstrates that the x-ray calibration technique works well to calibrate SRFs since CPS has been shown to be well characterized and calibrated[20]. In order to forward fit other spectra besides Gaussians, the user simply needs to change the input to the SRF Monte-Carlo toolkit. The SRF Monte-Carlo toolkit is needed for the use of MCMC techniques.

TABLE II. Comparison between the DD-p mean energies measured with x-ray calibrated SRFs and CPS. The Monte-Carlo toolkit is used to remove the instrument response from the SRF data allowing for direct comparison between SRF and CPS measurements.

Shot number	SRF mean energy (MeV)	CPS mean energy (MeV)
1	$2.83 \pm .158$	2.88 ± 0.101
2	$3.00 \pm .099$	3.10 ± 0.101
3	$3.08 \pm .083$	3.08 ± 0.101

VII. CONCLUSION

SRFs play an important role in ICF and stellar nucleosynthesis experiments. They are physically constructed by overlaying filters of different thicknesses together and use CR-39 as their detection medium. Charged particles are slowed down by the SRF filters and produce tracks on the CR-39. A charged-particle spectrum, convolved with the instrument response function, is reconstructed by comparing the spectra inferred from each SRF window.

The ability to customize the energy range for detecting specific nuclear reaction products sets the SRF apart from other diagnostics. Since a large number of parameters can be varied, it is necessary to be able to predict the performance of a given SRF design before detector construction and usage. The SRF Monte-Carlo toolkit presented herein provides a unique capability of testing out new SRF designs and exploring the various subtleties of the data analysis. The toolkit also inherently encodes the SRF instrument response function which is important for any use of the SRF.

The SRF Monte-Carlo toolkit, using Geant4, was built to generate synthetic SRF data in order to validate SRF designs and study the instrument response function. Geant4 is used to simulate the ranging of protons through each SRF window. The physics lists used accounts for normal stopping power as well as energy straggling through the use of a Coulomb scattering model. The resulting proton spectrum is recorded for each SRF window. Proton energies are converted into diameters on the CR-39 and diameter blurring is applied. The resulting diameter distribution is subsequently fed into the usual SRF solver to generate a synthetic SRF spectrum.

This Monte-Carlo toolkit was applied to study several features of different SRF designs. A new ^{3}He^{3}He-p SRF design was validated and an analysis method was put forth to analyze experimental data which accounts for the instrument response. It was also shown that a filter-thickness calibration better than 5% precision is required to accurately measure the ^{3}He^{3}He-p spectrum. This level of precision is possible using an x-ray calibration technique. The code was also applied to validate an SRF design for the CRS spectrometer. Lastly, a new x-ray calibration technique is shown to work well through a comparison between SRF and CPS measurements of OMEGA implosions.

The SRF Monte-Carlo toolkit provides a unique capability to validate any detector before construction and deployment. The usability of the code enables future studies into the intricacies of the SRF as a diagnostic as well as accurate analysis

of unique data that only the SRF is able to obtain.

ACKNOWLEDGMENTS

The authors would like to thank R. Frankel and E. Doeg for help with processing the CR-39 used herein. The authors also thank the peer-reviewers for their insightful comments. This work was supported in part by the U.S. Department of Energy NNSA MIT Center-of-Excellence under Contract DE-NA0003868. This report was prepared as an account of work sponsored by an agency of the United States Government. Neither the United States Government nor any agency thereof, nor any of their employees, makes any warranty, express or implied, or assumes any legal liability or responsibility for the accuracy, completeness, or usefulness of any information, apparatus, product, or process disclosed, or represents that its use would not infringe privately owned rights. Reference herein to any specific commercial product, process, or service by trade name, trademark, manufacturer, or otherwise does not necessarily constitute or imply its endorsement, recommendation, or favoring by the United States Government or any agency thereof. The views and opinions of authors expressed herein do not necessarily state or reflect those of the United States Government or any agency thereof.

Appendix A: Validation of modified Geant4 using SRIM

While TRIM is considered the "gold-standard" for cold matter stopping power calculations, it would be very difficult to use for the SRF Monte-Carlo toolkit[11]. TRIM is not multithreaded and is very slow in comparison to Geant4 all the while forcing the user to use a graphical user interface. The TRIM input spectra are limited to mono-energetic lines. All of these factors make TRIM ill-suited for Monte-Carlo work at the scale necessary for SRF validation. As stated in the main text, the Geant4 physics list used in the toolkit was modified to use SRIM stopping power to produce more accurate results. In this appendix, the SRIM modified Geant4 physics list is compared to TRIM as well as the `emstandardSS` physics list.

Fig. 9 shows the DD-p SRF mean energy response curve for synthetic SRF data generated with TRIM and the SRIM modified Geant4 physics list generated with a mono-energetic 3.0 MeV proton spectrum. The results show that the SRF response is within errorbars at this low energy of 3 MeV. This is expected since there is not enough thickness for the differences in the Coulomb scattering models between TRIM and Geant4 to manifest. Therefore, for low energy SRFs, there is a negligible difference between TRIM and the Geant4 physics list used in the Monte-Carlo toolkit.

For high energy particles, the differences between the models is more apparent. Fig. 10 shows the output proton spectra from the different Monte-Carlo codes for a mono-energetic 10.0 MeV proton spectrum ranged through 150 μm, 180 μm, and 190 μm of Ta. The comparison here also includes the `emstandardSS` physics list. Tabulated spectral quantities are shown in Tab. III. In both the figure and table, it is clear

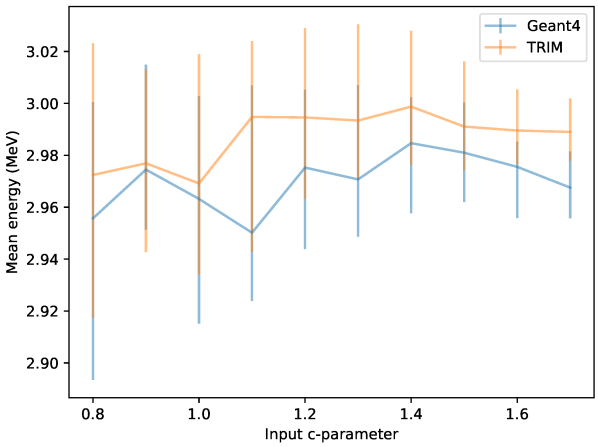

FIG. 9. SRF mean energy shift response from both TRIM and the Geant4 physics list modified to use SRIM for stopping power. The data were generated using a 3 MeV mono-energetic proton spectrum.

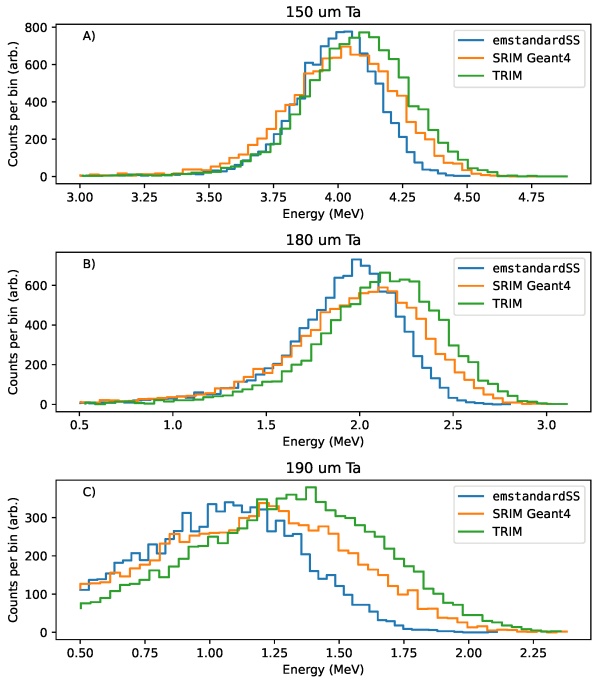

FIG. 10. Comparison between the output spectra generated by ranging 10 MeV protons through A) 150 μm, B) 180 μm, and C) 190 μm tantalum using TRIM, Geant4 using the `emstandardSS` physics list, and the Geant4 physics list using SRIM stopping power.

that the SRIM modified physics list is closer to the TRIM output than the `emstandardSS` physics list. The SRIM modified physics list mean energies are still larger than TRIM, but the widths are quite similar. This comparison shows that using the modified Geant4 physics list produces results more similar to

TABLE III. Comparison of spectral quantities for the different models. The table shows the mean energies and spectral widths of the spectra shown in Fig. 10.

	Foil thickness	`emstandardSS`	SRIM	Geant4	TRIM
Mean (MeV)	150 μm	4.015	4.042	4.106
	180 μm	1.947	2.019	2.145
	190 μm	1.085	1.214	1.328
Width (MeV)	150 μm	0.176	0.224	0.212
	180 μm	0.224	0.383	0.353
	190 μm	0.212	0.355	0.363

TRIM than the built-in Geant4 physics lists.

Appendix B: Comparison between ^{3}He^{3}He-p SRF designs

Window overlap is essential for the SRF to provide high-fidelity data. An SRF analysis fails when the maximum measurable energy of one window is a few energy bins below the minimum measurable energy of the window with a filter thickness one step above[2]. This appendix compares the energy overlap of the new ^{3}He^{3}He-p SRF to the old design. The new design has a window thickness step size of 15 μm while the old design has a step size of 25 μm. Both designs had a base filter of 10 μm. When analyzing SRF data, minimum and maximum diameters are chosen to exclude ranged-out tracks as well as underdeveloped tracks. In normal operation, these numbers tend to be $D_{\max} = 17$ μm and $D_{\min} = 9$ μm. In more extreme cases, smaller diameters down to 4 μm can be allowed. Below about 4 μm, the tracks are underdeveloped and should not be used. The minimum and maximum energies within an SRF window can be described by:

$$E_{\min,i} = E_{\text{in}}(E(D_{\max}, c), T_i) \quad \text{(B.1)}$$

$$E_{\max,i} = E_{\text{in}}(E(D_{\min}, c), T_i) \quad \text{(B.2)}$$

where E_{in} is the SRIM[11] stopping power function which reverse ranges a particle of a given energy through material of thickness T, T_i is the thickness of the i-th filter, and c is the c-parameter. The SRF fails to provide high-fidelity data when $E_{\min,i+1} + dE > E_{\max,i} - dE$. Here, dE is the size of the spectral energy bin. At least two overlapping energy bins are required to make a successful SRF analysis as shown in Fig. 11. In Fig. 11 A), a plot of $E_{\max,0}$ alongside $E_{\min,1}$ is shown for both the new and old SRF designs as a function of the c-parameter. As stated earlier, the analysis fails when $E_{\min,1}$ exceeds $E_{\max,0}$ by a few energy bins. The point of failure is where the curves meet. Comparing the two SRF designs, it is clear that the new 16 window SRF will work at larger c-parameters than the 9 window SRF. Note that the new design is not guaranteed to always work; there does exist some c-parameters which it will fail. The additional energy overlap between SRF windows in the new design makes it much more likely that the SRF will produce good results in experiments.

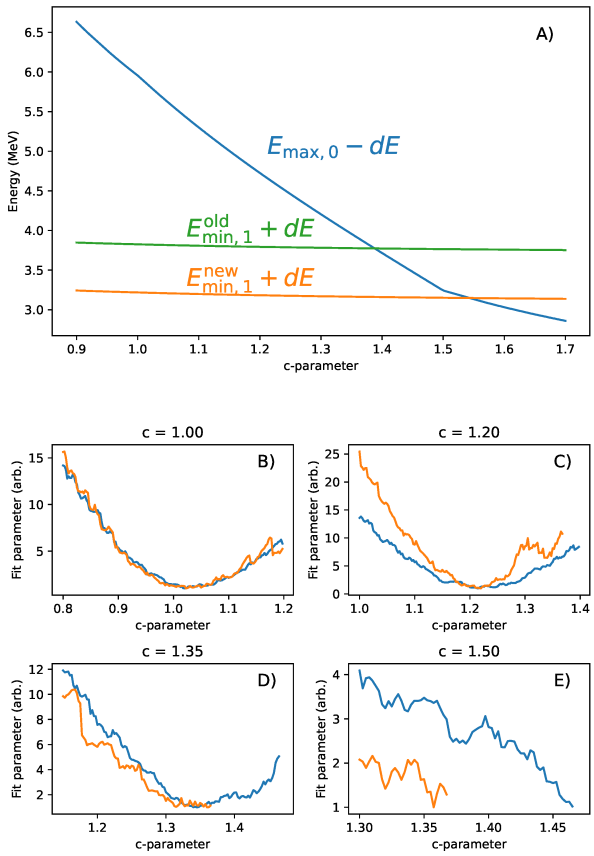

FIG. 11. A) SRF window energy overlap between the new and old SRF designs as a function of c-parameter. The blue is the maximum energy of the thinnest SRF window for both designs (10 μm). The orange (green) is the minimum energy of second thinnest SRF window for the new (old) ^{3}He^{3}He-p SRF design. This is the point where the blue curve meets the orange and green curves. At c-parameters higher than this, there is no overlap and the SRF analysis fails. B)-E) SRF fit parameter curves for the new (blue) and old (orange) SRF designs. The SRF analysis fails at c-parameters above where the plot stops. This is seen in subfigure D) where the orange curve stops at $c \sim 1.35$. The new SRF design is shown to work over a larger range of c-parameters.

The failure of the SRFs to provide high-fidelity data at large c-parameters is confirmed by SRF Monte-Carlo simulations. Synthetic ^{3}He^{3}He-p spectra are generated with the MC code for different c-parameters and the fit parameter as a function of c-parameter is shown in Fig. 11 B-E). The fit parameter is described elsewhere but put simply, it quantifies how much individual SRF windows agree with each other[2]. The correct c-parameter is the one where the fit parameter is at a global and local minimum. The SRF analysis procedure fails when there is no minimum as seen in Fig. 11 D) and E). The figures show that the new SRF design outperforms the old one by working at higher c-parameter. It is essential to maximize the allowable range of c-parameters since it is unknown, prior to etching, what c-parameter will apply to the piece of CR-39 fielded in an experiment.

Appendix C: Variability of SRF response

The response function of the SRF is complicated and depends on many parameters. In previous work, the response has been decomposed into a shift and broadening of the spectrum[2]. Not only does this depend on the c-parameter of the CR-39 and the input energy, the response also depends on the number of filters used for the analysis. Fig. 12 shows the mean energy shift of a 3.0 MeV mono-energetic DD proton spectrum inferred from the synthetic SRF data versus c-parameter for different number of windows. For the chosen input c-parameters, all of these filter combinations provide high-fidelity data without ranging issues for the thicker filters. This is reflected by the analysis with the four windows not being done at small c-parameter. The figure shows that the energy shift can be more than 100 keV, depending on the number of windows. The large error bars, a result of nominal SRF fluence, adds additional uncertainty in the SRF response when fewer windows are used.

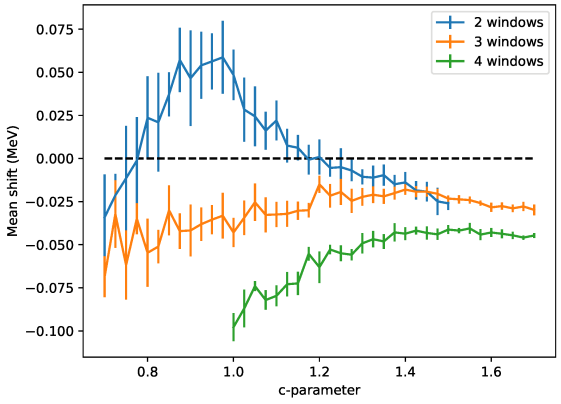

FIG. 12. Mean energy shift of a 3.0-MeV mono-energetic DD proton spectrum inferred from the synthetic SRF data versus c-parameter for different numbers of windows. The tantalum filtering used in these simulations were (10 μm, 15 μm), (10 μm, 15 μm, 20 μm), and (10 μm, 15 μm, 20 μm, 25 μm). Note that the four-window data is not generated at small c-parameters. This is because the thickest window does not overlap well with the other windows. In a real analysis, one would just neglect the thickest filter at small c-parameters.

The variability of the SRF response precludes using a single instrumentation response function for the forward fitting approach. Instead, analysis methods like the one described for the SRF ^{3}He^{3}He-p in section IV or for the DD-p SRF in section VI are required.

DATA AVAILABILITY

The data that support the findings of this study are available from the corresponding author upon reasonable request.

REFERENCES

[1] M. J. Rosenberg, A. B. Zylstra, J. A. Frenje, H. G. Rinderknecht, M. G. Johnson, C. J. Waugh, F. H. Séguin, H. Sio, N. Sinenian, C. K. Li, and et al., Rev. Sci. Instrum. **85**, 103504 (2014).

[2] B. Lahmann, M. G. Johnson, J. A. Frenje, A. J. Birkel, P. J. Adrian, N. Kabadi, J. H. Kunimune, T. M. Johnson, J. A. Pearcy, B. L. Reichelt, and et al., Rev. Sci. Instrum. **92**, 083506 (2021).

[3] F. H. Séguin, J. A. Frenje, C. K. Li, D. G. Hicks, S. Kurebayashi, J. R. Rygg, B.-E. Schwartz, R. D. Petrasso, S. Roberts, J. M. Soures, and et al., Rev. Sci. Instrum. **74**, 975 (2003).

[4] A. B. Zylstra, J. A. Frenje, M. Gatu Johnson, G. M. Hale, C. R. Brune, A. Bacher, D. T. Casey, C. K. Li, D. McNabb, M. Paris, and et al., Phys. Rev. Lett. **119** (2017).

[5] S. Agostinelli, J. Allison, K. Amako, J. Apostolakis, H. Araujo, P. Arce, M. Asai, D. Axen, S. Banerjee, G. Barrand, and et al., Nucl. Instrum. Methods Phys. Res. A **506**, 250 (2003).

[6] J. Allison, K. Amako, J. Apostolakis, H. Araujo, P. Arce Dubois, M. Asai, G. Barrand, R. Capra, S. Chauvie, R. Chytracek, and et al., IEEE Trans. Nucl. Sci. **53**, 270 (2006).

[7] J. Allison, K. Amako, J. Apostolakis, P. Arce, M. Asai, T. Aso, E. Bagli, A. Bagulya, S. Banerjee, G. Barrand, and et al., Nucl. Instrum. Methods Phys. Res. A **835**, 186 (2016).

[8] B. Lahmann, M. Gatu Johnson, K. D. Hahn, J. A. Frenje, D. J. Ampleford, B. Jones, M. A. Mangan, A. Maurer, C. L. Ruiz, F. H. Séguin, and et al., Rev. Sci. Instrum. **91**, 073501 (2020).

[9] F. H. Seguin, N. Sinenian, M. Rosenberg, A. Zylstra, M. J.-E. Manuel, H. Sio, C. Waugh, H. G. Rinderknecht, M. G. Johnson, J. Frenje, and et al., Rev. Sci. Instrum. **83**, 10D908 (2012).

[10] B. Lahmann, M. Gatu Johnson, J. A. Frenje, Y. Y. Glebov, H. G. Rinderknecht, F. H. Séguin, G. Sutcliffe, and R. D. Petrasso, Rev. Sci. Instrum. **91**, 053502 (2020).

[11] J. F. Ziegler, Nucl. Instrum. Methods Phys. Res. B **219-220**, 1027 (2004).

[12] N. Sinenian, M. J.-E. Manuel, A. B. Zylstra, M. Rosenberg, C. J. Waugh, H. G. Rinderknecht, D. T. Casey, H. Sio, J. K. Ruszczynski, L. Zhou, and et al., Rev. Sci. Instrum. **83**, 043502 (2012).

[13] C. Wong, J. D. Anderson, and J. W. McClure, Nucl. Phys. **71**, 106 (1965).

[14] C. R. Brune, J. A. Caggiano, D. B. Sayre, A. D. Bacher, G. M. Hale, and M. W. Paris, Phys. Rev. C Nucl. Phys. **92** (2015).

[15] D. B. Sayre, C. R. Brune, J. A. Caggiano, V. Y. Glebov, R. Hatarik, A. D. Bacher, D. L. Bleuel, D. T. Casey, C. J. Cerjan, M. J. Eckart, and et al., Phys. Rev. Lett. **111**, 052501 (2013).

[16] J. Pearcy, N. Kabadi, A. Birkel, P. Adrian, B. Lahmann, B. Reichelt, T. M. Johnson, G. Sutcliffe, J. Kunimune, M. Gatu-Johnson, and et al., Review of Scientific Instruments **92** (2021), 10.1063/5.0043770.

[17] J. A. Frenje, D. T. Casey, C. K. Li, F. H. Séguin, R. D. Petrasso, V. Y. Glebov, P. B. Radha, T. C. Sangster, D. D. Meyerhofer, S. P. Hatchett, and et al., Phys. Plasmas **17**, 056311 (2010).

[18] D. T. Casey, J. A. Frenje, M. G. Johnson, F. H. Séguin, C. K. Li, R. D. Petrasso, V. Y. Glebov, J. Katz, J. Magoon, D. D. Meyerhofer, and et al., Review of Scientific Instruments **84** (2013), 10.1063/1.4796042.

[19] D. G. Hicks, C. K. Li, R. D. Petrasso, F. H. Séguin, B. E. Burke, J. P. Knauer, S. Cremer, R. L. Kremens, M. D. Cable, and T. W. Phillips, Rev. Sci. Instrum. **68**, 589 (1997).

[20] P. J. Adrian, J. Armstrong, A. Birkel, C. Chang, S. Dannhoff, T. Evans, M. G. Johnson, T. M. Johnson, N. Kabadi, J. Kunimune, and et al., Rev. Sci. Instrum. **93**, 113534 (2022).